PAPER

A Pseudo Multi-Exposure Fusion Method Using Single Image

Yuma KINOSHITA†, *Student Member*, Sayaka SHIOTA†, *Member*, *and* Hitoshi KIYA†, *Fellow*

SUMMARY This paper proposes a novel pseudo multi-exposure image fusion method based on a single image. Multi-exposure image fusion is used to produce images without saturation regions, by using photos with different exposures. However, it is difficult to take photos suited for the multi-exposure image fusion when we take a photo of dynamic scenes or record a video. In addition, the multi-exposure image fusion cannot be applied to existing images with a single exposure or videos. The proposed method enables us to produce pseudo multi-exposure images from a single image. To produce multi-exposure images, the proposed method utilizes the relationship between the exposure values and pixel values, which is obtained by assuming that a digital camera has a linear response function. Moreover, it is shown that the use of a local contrast enhancement method allows us to produce pseudo multi-exposure images with higher quality. Most of conventional multi-exposure image fusion methods are also applicable to the proposed multi-exposure images. Experimental results show the effectiveness of the proposed method by comparing the proposed one with conventional ones.

key words: *Multi-Exposure Image Fusion, Image Enhancement, Contrast Enhancement, Tone Mapping*

1. Introduction

The low dynamic range (LDR) of the imaging sensors used in modern digital cameras is a major factor preventing cameras from capturing images as good as those with human vision. For this reason, the interest of high dynamic range (HDR) imaging has recently been increasing. Various research works on HDR imaging have so far been reported [1–8]. The research works are classified into two categories. The first one aims to generate HDR images having an extremely wide dynamic range. However, HDR display devices are not popular yet due to the high cost of the technologies. Hence, the second one focuses on tone mapping operations which generate standard LDR images from HDR ones [9–11]. Consequently, in order to generate high quality LDR images via HDR images, it is necessary not only to generate HDR ones but also to map them into LDR ones.

To generate LDR images more simply, multi-exposure image fusion methods have been proposed [12–18]. The reported fusion methods use a stack of differently exposed images, "multi-exposure images," and fuse them to produce an image with high quality. The advantage of these methods, compared with the ones via HDR images, is that they eliminate three operations: generating HDR images, calibrating a camera response function (CRF), and preserving the exposure value of each photograph. However, the conventional multi-exposure image fusion methods have several problems due to the use of a stack of differently exposed images. If the scene is dynamic or the camera moves while pictures are being captured, the multi-exposure images in the stack will not line up properly with one another. This misalignment results in ghost-like artifacts in the fused image. Although a number of methods have been proposed [4, 16] to eliminate these artifacts, the effectiveness of these methods is limited because it is difficult to apply them to videos. In addition, multi-exposure image fusion methods cannot be applied to existing images with a single exposure or videos.

Because of such a situation, this paper proposes a novel pseudo multi-exposure image fusion method using a single image. The proposed method enables us to produce pseudo multi-exposure images from a single image and to improve the image quality by fusing them. To produce multi-exposure images, the proposed method use the relationship between the exposure values and pixel values, which is obtained by assuming that a digital camera has a linear response function. Moreover, the use of a local contrast enhancement method improves the quality of the pseudo multi-exposure images. Most of conventional multi-exposure image fusion methods are also applicable to the proposed pseudo multi-exposure images. Furthermore, the proposed method is useful for both reducing the number of input images used in conventional fusion ones, and improving the quality of multi-exposure images.

We evaluate the effectiveness of the proposed method in terms of the quality of generated images by a number of simulations. In the simulations, the proposed method is compared with existing multi-exposure image fusion methods and typical contrast enhancement methods. The results show that the proposed method can produce high quality images, as well as conventional fusion methods with multi-exposure images. In addition, the proposed method outperforms typical contrast enhancement methods in terms of the color distortion.

Manuscript received January 1, 2011.
Manuscript revised January 1, 2011.
†Department of Information and Communication Systems, Tokyo Metropolitan University, 191-0065, Tokyo, Japan
DOI: 10.1587/transfun.E0.A.1

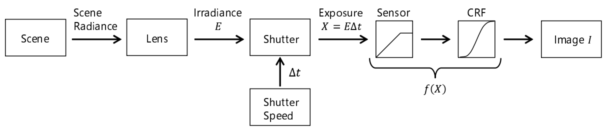

Fig. 1 Imaging pipeline of digital camera

2. Preparation

Multi-exposure fusion methods use images taken under different exposure conditions, i.e., multi-exposure images. Here we discuss the relationship between exposure values and pixel values. For simplicity, we focus on grayscale images.

2.1 Relationship between exposure values and pixel values

Figure 1 shows the imaging pipeline for a digital camera [19]. The radiant power density at the sensor, i.e., irradiance E, is integrated over the time Δt the shutter is open, producing an energy density, commonly referred to as exposure X. If the scene is static during this integration, exposure X can be written simply as the product of irradiance E and integration time Δt (referred to as "shutter speed"):

$$X(p) = E(p)\Delta t, \tag{1}$$

where $p = (x, y)$ indicates the pixel at point (x, y). A pixel value $I(p) \in [0, 1]$ in the output image I is given by

$$I(p) = f(X(p)), \tag{2}$$

where f is a function combining sensor saturation and a camera response function (CRF). The CRF represents the processing in each camera which makes the final image $I(p)$ look better.

Camera parameters, such as shutter speed and lens aperture, are usually calibrated in terms of exposure value (EV) units, and the proper exposure for a scene is automatically selected by the camera. The exposure value is commonly controlled by changing the shutter speed although it can also be controlled by adjusting various camera parameters. Here we assume that the camera parameters except for the shutter speed are fixed. Let 0[EV] and $\Delta t_{0\mathrm{EV}}$ be the proper exposure value and shutter speed under the given conditions, respectively. The exposure value v_i[EV] of an image taken at shutter speed Δt_i is derived from

$$v_i = \log_2 \Delta t_i - \log_2 \Delta t_{0\mathrm{EV}}. \tag{3}$$

From eq. (1) to eq. (3), images $I_{0\mathrm{EV}}$ and I_i exposed at 0[EV] and v_i[EV], respectively, are written as

$$I_{0\mathrm{EV}}(p) = f(E(p)\Delta t_{0\mathrm{EV}}) \tag{4}$$

$$I_i(p) = f(E(p)\Delta t_i) = f(2^{v_i} E(p)\Delta t_{0\mathrm{EV}}). \tag{5}$$

Assuming function f is linear, we obtain the following relationship between $I_{0\mathrm{EV}}$ and I_i:

$$I_i(p) = 2^{v_i} I_{0\mathrm{EV}}(p). \tag{6}$$

Therefore, the exposure can be varied artificially by multiplying $I_{0\mathrm{EV}}$ by a constant. This ability is used in our proposed pseudo multi-exposure fusion method, which is described in the next section.

3. Proposed pseudo multi-exposure image fusion

In this paper, we propose a novel pseudo multi-exposure image fusion method which fuses multi-exposure images generated form a single image. The outline of the proposed method is shown in Fig. 2. In the proposed method, local contrast enhancement is applied to the luminance L calculated from the original image I and then pseudo exposure compensation and tone mapping are also applied. Next, image I' with improved quality is produced by multi-exposure image fusion.

3.1 Local contrast enhancement

If pseudo multi-exposure images are generated form a single image, the quality of an image fused from them will be lower than that of an image fused from genuine multi-exposure images. Therefore, the dodging and burning algorithm is used to enhance the local contrast [20]. The algorithm is given by

$$L_c(p) = \frac{L^2(p)}{L_a(p)}, \tag{7}$$

where $L_a(p)$ is the local average of luminance $L(p)$ around pixel p. It is obtained by applying a low-pass filter to $L(p)$. Here, a bilateral filter is used for this purpose.

$L_a(p)$ is calculated using the bilateral filter

$$L_a(p) = \frac{1}{c(p)} \sum_{q \in \Omega} L(q) g_{\sigma_1}(q - p) g_{\sigma_2}(L(q) - L(p)), \tag{8}$$

where Ω is the set of all pixels, and $c(p)$ is a normalization term such as

$$c(p) = \sum_{q \in \Omega} g_{\sigma_1}(q - p) g_{\sigma_2}(L(q) - L(p)), \tag{9}$$

where g_σ is a Gaussian function given by

$$g_\sigma(p|p = (x, y)) = C_\sigma \exp\left(-\frac{x^2 + y^2}{\sigma^2}\right) \tag{10}$$

using a normalization factor C_σ. Parameters $\sigma_1 = 16, \sigma_2 = 3/255$ are set in accordance with [20].

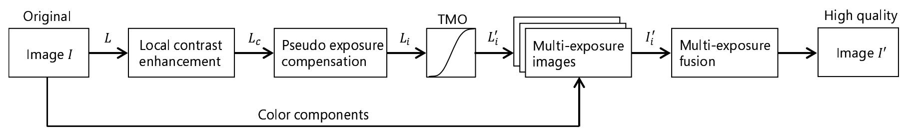

Fig. 2 Outline of proposed method

3.2 Pseudo exposure compensation

The pseudo exposure compensation consists of two steps: estimating luminance $L_{0\mathrm{EV}}$ from L_c and calculating luminance $L_i (1 \leq i \leq N, i \in \mathbb{N})$ of the ith image, where $L_{0\mathrm{EV}}$ is the luminance of the properly exposed image i.e. with 0[EV], and N is the number of pseudo multi-exposure images produced by the proposed method.

In the first step, there are two approaches A and B to estimate the luminance $L_{0\mathrm{EV}}$. Approach A estimates $L_{0\mathrm{EV}}$ on the basis of automatic exposure algorithms in digital cameras, so that it enables us to avoid color distortions between a resulting image and the original image. On the other hand, approach B estimates $L_{0\mathrm{EV}}$ by using all luminance values of the scene unlike the automatic exposure algorithms which generally use luminance values in specific area of the scene. Hence, approach B allows us to strongly enhance the contrast in all image regions. Note that approach A is only available when the exposure value v[EV] of the original image I is known. In contrast, approach B is available regardless whether the exposure value v[EV] of I is known or not.

A. Estimating $L_{0\mathrm{EV}}$ with exposure value v
In approach A, according to eq. (6), $L_{0\mathrm{EV}}$ is estimated as

$$L_{0\mathrm{EV}}(p) = 2^{-v} L_c(p). \tag{11}$$

B. Estimating $L_{0\mathrm{EV}}$ without exposure value v
In approach B, we map the geometric mean $\overline{L}_c$ of luminance L_c to middle-gray of the displayed image, or 0.18 on a scale from zero to one, as in [21], where the geometric mean of the luminance values indicates the approximate brightness of the image.

The luminance $L_{0\mathrm{EV}}$ is derived from

$$L_{0\mathrm{EV}}(p) = \frac{0.18}{\overline{L}_c} L_c(p) \tag{12}$$

where the geometric mean $\overline{L}_c$ of $L_c(p)$ is calculated using

$$\overline{L}_c = \exp\left(\frac{1}{|\Omega|}\sum_{p\in\Omega} \log L_c(p)\right). \tag{13}$$

If eq. (13) has singularities at some pixels i.e. $L_c(p) = 0$, $\overline{L}_c$ is calculated by

$$\overline{L}_c = \exp\left(\frac{1}{|\Omega|}\left(\sum_{p\notin B} \log L_c(p) + \sum_{p\in B} \log \epsilon\right)\right) \tag{14}$$

where $B = \{p | L_c(p) = 0\}$ and ϵ is a small value.

The second step of the pseudo exposure compensation is carried out according to eq. (6). The luminance L_i of the ith image I_i is obtained by

$$L_i(p) = 2^{v_i} L_{0\mathrm{EV}}(p), \tag{15}$$

so that the image I_i could have the exposure value v_i[EV]. To generate high quality images, multi-exposure images should represent bright, middle and dark regions of the original image I, respectively. Since the image having 0[EV] represents the middle region clearly, a negative value, zero and a positive value should be used as the parameters v_i. In this paper, we use $N = 3$, and $v_i = -1, 0, +1$[EV].

3.3 Tone mapping

Since the luminance value $L_i(p)$ calculated by the pseudo exposure compensation often exceeds the maximum value of the common image format. Pixel values might be lost due to truncation of the values. This problem is overcome, by using a tone mapping operation to fit the luminance value into the interval $[0, 1]$.

The luminance L'_i of a pseudo multi-exposure image is obtained, by applying a tone mapping operator F_i to L_i:

$$L'_i(p) = F_i(L_i(p)). \tag{16}$$

Reinhard's global operator is used here as tone mapping operator F_i [21].

Reinhard's global operator is given by

$$F_i(L(p)) = \frac{L(p)\left(1 + \frac{L(p)}{L^2_{white_i}}\right)}{1 + L(p)}, \tag{17}$$

where parameter $L_{white_i} > 0$ determines luminance value $L(p)$ as $L'(p) = F_i(L(p)) = 1$. Note that Reinhard's global operator F_i is a monotonically increasing function. Here, let $L_{white_i} = \max L_i(p)$. We obtain $L'_i(p) \leq 1$ for all p. Therefore, truncation of the luminance values can be prevented.

Combining L'_i, luminance L of the original image I, and RGB pixel values $C(p) \in \{R(p), G(p), B(p)\}$ of I, we obtain RGB pixel values $C'_i(p) \in \{R'_i(p), G'_i(p), B'_i(p)\}$ of pseudo multi-exposure images

I'_i:

$$C'_i(p) = \frac{L'_i(p)}{L(p)} C(p). \tag{18}$$

3.4 Fusion of pseudo multi-exposure images

Pseudo multi-exposure images I'_i can be used as input for any multi-exposure image fusion method. While numerous methods for fusing images have been proposed, here we use those of Mertens et al. [13], Sakai et al. [17], and Nejati et al. [18]. A final image I' is produced using

$$I' = \mathscr{F}(I'_1, I'_2, \cdots, I'_N), \tag{19}$$

where $\mathscr{F}(I_1, I_2, \cdots, I_N)$ indicates a function to fuse N images $I_1, I_2, \cdots, I_N$ into a single image.

3.5 Proposed procedure

The procedure for generating an image I' from the original image I by the proposed method is summarized as follows (see Fig. 2).

1. Calculate luminance L of the original image I.
2. Calculate L_c by using eq. (7) to eq. (10).
3. Calculate L_i according to eq. (15).
   Approach A. Calculate $L_{0\mathrm{EV}}$ by eq. (11).
   Approach B. Calculate $L_{0\mathrm{EV}}$ by eqs. (12) and (14).
4. Calculate luminance values L'_i of pseudo multi-exposure images I'_i from eqs. (16) and (17).
5. Generate I'_i according to eq. (18).
6. Obtain an image I' with a multi-exposure image fusion method $\mathscr{F}$ as in eq. (19).

4. Simulation

Using two simulations, "Simulation 1" and "Simulation 2," we evaluated the quality of the images produced by the proposed method, the three fusion methods mentioned above, and typical single image based contrast enhancement methods, i.e. the histogram equalization (HE), the contrast limited adaptive histograph equalization (CLAHE) [22], and the contrast-accumulated histogram equalization (CACHE) [23].

4.1 Comparison with conventional methods

To evaluate the quality of the images produced by each method, objective metrics are needed. Typical metrics such as the peak signal to noise ratio (PSNR) and the structural similarity index (SSIM) are not suitable for this purpose because they use the target image with the highest quality as a reference one. We therefore used TMQI [24] and CIEDE2000 [25] as the metrics as they do not require any reference images.

TMQI represents the quality of images tone mapped from an HDR image; the index incorporates structural fidelity and statistical naturalness. An HDR image is used as a reference to calculate structural fidelity. Any references are not needed to calculate statistical naturalness. Since the processes of tone mapping and photographing are similar, TMQI is also useful for evaluating photographs. CIEDE2000 represents the distance in a color space between two images. We used CIEDE2000 to evaluate the color distortion caused by the proposed method.

4.2 Simulation conditions

4.2.1 Simulation 1 (using HDR images)

In Simulation 1, HDR images were used to prepare the input images for the proposed method. The following procedure was carried out to evaluate the effectiveness of the proposed method.

1. Map HDR image I_H to three multi-exposure images $I_{Mk}, k = 1, 2, 3$ with exposure values $v_{Mk} = k - 2$[EV] by using a tone mapping operator (see Fig. 3).
2. Obtain I' from I according to the proposed procedure as in 3.5, under $I = I_{M2}$ having $v_{M2} = 0$[EV].
3. Compute TMQI values between I' and I_H.
4. Compute CIEDE2000 values as an error measure between I' and I_{M2}.

In step 1), the tone mapping operator corresponds to function f in eqs. (4) and (5) (see Fig. 1). As assumed for eq. (6), a linear operator was used as the tone mapping operator. In addition, the properly exposed image, having 0[EV], for each scene was defined as an image in which the geometric mean of the luminance equals to 0.18.

We used 60 HDR images selected from available online databases [26, 27].

4.2.2 Simulation 2 (photographing directly)

In Simulation 2, four photographs taken by Canon EOS 5D Mark II camera and eight photographs selected from an available online database [28] were directly used as input images I_{Mk} (see Fig. 4). Since there were no HDR images for Simulation 2, the first step in Simulation 1 was not needed. In addition, structural fidelity in TMQI could not be calculated due to the non-use of HDR images. Thus, we used only statistical naturalness in TMQI as a metric.

4.3 Simulation results

Here, the effectiveness of the proposed method is discussed on the basis of objective assessments.

4.3.1 Simulation 1

Tables 1, 2 and 3 summarize TMQI score, statistical

(a) I_{M1} ($v_{M1} = -1$[EV]) (b) I_{M2} ($v_{M2} = 0$[EV]) (c) I_{M3} ($v_{M3} = +1$[EV])

Fig. 3 Examples of multi-exposure images I_{Mk} (Memorial) mapped from I_H

(a) I_{M1} ($v_{M1} = -1.3$[EV]) (b) I_{M2} ($v_{M2} = 0$[EV]) (c) I_{M3} ($v_{M3} = +1.3$[EV])

Fig. 4 Examples of multi-exposure images I_{Mk} (Estate rsa) for Simulation 2

naturalness score, and CIEDE2000 score for Simulation 1, respectively. For TMQI $\in [0, 1]$ (and statistical naturalness $\in [0, 1]$), a larger value means higher quality. For CIEDE2000 $\in [0, \infty)$, a smaller value intends that the color difference between two images is smaller.

a) Comparison with multi-exposure fusion methods
Table 1 shows the results of evaluating three multi-exposure fusion methods (MEF), three conventional contrast enhancement methods (CE), and the proposed method, in terms of TMQI, where the proposed method has six variations. Here CE and the proposed method utilized a single image I_{M2} having 0[EV] as the input image, although MEF used three multi-exposure images I_{M1}, I_{M2} and I_{M3} as input ones. By comparing MEF with approach A and B (e.g. comparing MEF [13] with the proposed method using [13]), it is confirmed that both approach A and B provide higher TMQI scores than MEF, even though the proposed ones used a single image as an input image. Statistical naturalness scores (in Table 2) also show a similar trend to Table 1.

By considering CIEDE2000 scores in Table 3, it is also confirmed that approach A has better CIEDE scores than MEF.

Figure 5 shows an example of images generated by each method. In this figure, the results of approach A are not shown because there were few visual differences between approach A and approach B. This is because exposure values of input images were determined in the same way as that utilized in approach B for estimating $L_{0\text{EV}}$ (given by eq. 12), in Simulation 1. From the figure, it is confirmed that the proposed method can produce an image with almost the same as ones fused by MEF.

These results demonstrate that the proposed method is effective as well as MEF. Moreover, CIEDE2000 scores denote that approach A can produce images with higher quality, in terms of the color distortion, than approach B.

b) Comparison with contrast enhancement methods
Contrast enhancement also allows us to enhance the quality of images from a single image. To clearly show the effectiveness of the proposed method, we compared the proposed method with typical contrast enhancement methods.

Contrast enhancement methods provided higher TMQI and statistical naturalness scores than that of the proposed ones as shown in Tables 1 and 2. Especially, CACHE which is the state-of-the-art method has the best scores in all methods. However, they have the worst CIEDE2000 scores (see Table 3). The result means that the use of a contrast enhancement method would produce some serious color distortion. By comparing Fig. 5 with Fig. 3, it is also confirmed that contrast enhancement methods bring color distortion, e.g. the carpet on stairs (boxed by red line). In addition, since contrast enhancement methods aim to maximize image contrast, the resulting images sometimes have unnatural contrast due to over-enhancement (see regions boxed by blue line in Fig. 5). By contrast, the proposed method can prevent both the color distortion and the over-enhancement. Therefore, the proposed methods outperforms contrast enhancement methods in terms of the color distortion and the over-enhancement.

The results of Simulation 1 show that the proposed method enables us to produce high-quality images as well as conventional MEF, even when a single image is used as an input image. Besides, the proposed method also outperforms CE in therms of the color distortion and the over-enhancement. Comparison between approach A and B demonstrate that approach A can provide better CIEDE2000 scores than approach B, although approach B can strongly enhance the contrast of images as described later.

4.3.2 Simulation 2

In Simulation 2, statistical naturalness scores also show a similar trend to Simulation 1 (see Table 4). Besides, Table 5 shows that proposed methods using approach B as in 3.2 has worse CIEDE2000 scores than CLAHE and CACHE. This is due to the difference of estimating method for $L_{0\text{EV}}$ between digital cameras and the proposed method using approach B. In approach B, estimated $L_{0\mathrm{EV}}$ is differ from ones estimated by digital cameras. As a result, brightness of images produced by the proposed one using approach B is differ substantially from the input image as shown in Fig. 6. On the other hand, approach A enables us to avoid color distortions since it estimates $L_{0\mathrm{EV}}$ by using exposure values calculated by digital cameras. Thus, approach A has the lowest CIEDE2000 scores in the methods (see Table 5).

From Fig. 6, it is also confirmed that CE methods (He and CACHE) cause the loss of details in bright regions boxed by red line. This is due to the fact that these CE methods decrease the number of gradations assigned for bright regions, to enhance dark regions. By contrast, both approaches A and B can enhance images without the loss of details, as well as conventional MEF.

From these results, the proposed method enables us to generate images with high quality, as well as conventional MEF, from a single image. In addition, approach A outperforms typical contrast enhancement methods in terms of the color distortion. On the other hand, approach B can strongly enhance the contrast of images without loss of details, unlike conventional CE methods.

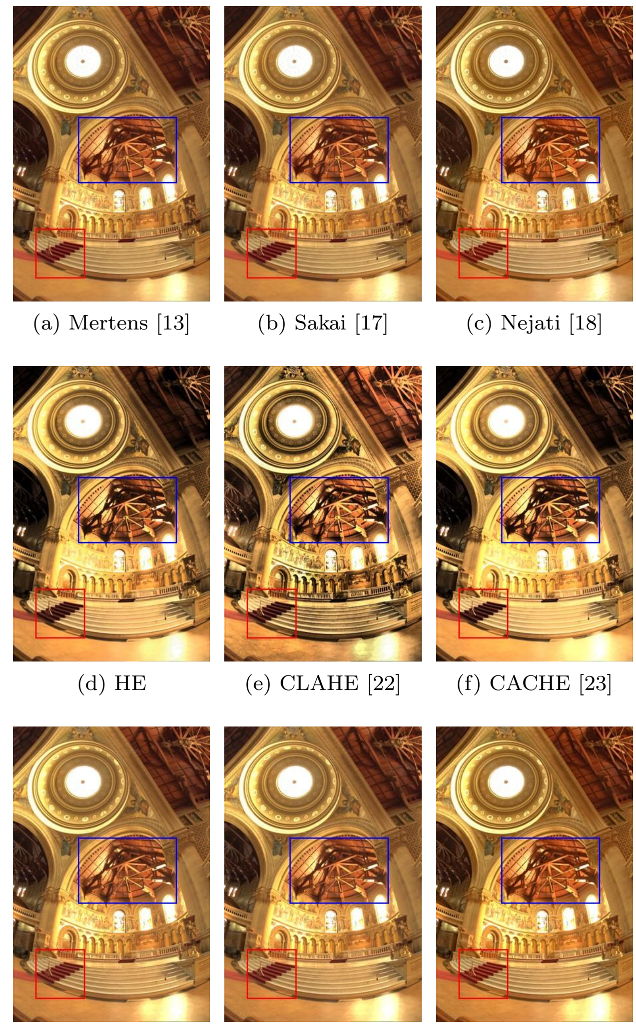

(a) Mertens [13] (b) Sakai [17] (c) Nejati [18]
(d) HE (e) CLAHE [22] (f) CACHE [23]
(g) Proposed (B) with [13] (h) Proposed (B) with [17] (i) Proposed (B) with [18]

Fig. 5 Images I' generated from image “Memorial”

5. Conclusion

Our proposed method produces pseudo multi-exposure images from a single image and the use of a local contrast enhancement method improves their quality. The proposed method is done by utilizing the relationship between the exposure values and pixel values. Approaches A and B used in the proposed method enables us to avoid color distortions and to strongly enhance the image contrast, respectively. Approach B is available even when the exposure value of an input image is unknown, while approach A is only available when the exposure value is known. Experimental results showed that the proposed method can effectively enhances images as well as conventional multi-exposure image fusion methods, without multi-exposure images. In addition, the proposed approach A outperforms typical contrast enhancement methods in terms of the color distortion. On the other hand, approach B allows us to strongly enhance the contrast of images without loss of details, unlike conventional contrast enhancement methods.

References

[1] M. Schöberl, J. Keinert, M. Ziegler, J. Seiler, M. Niehaus, G. Schuller, A. Kaup, and S. Foessel, “Evaluation of a high dynamic range video camera with non-regular sensor,” SPIE Electronic Imaging, pp.86600M–1–86600M–12, 2013.
[2] A. Chalmers, G. Bonnet, F. Banterle, P. Dubla, K. Debattista, A. Artusi, and C. Moir, “High-dynamic-range video solution,” ACM SIGGRAPH ASIA 2009 Art Gallery & Emerging Technologies: Adaptation, pp.71–71, ACM, 2009.
[3] P.E. Debevec and J. Malik, “Recovering high dynamic range radiance maps from photographs,” ACM SIGGRAPH, pp.369–378, ACM, 1997.
[4] T.H. Oh, J.Y. Lee, Y.W. Tai, and I.S. Kweon, “Robust high dynamic range imaging by rank minimization,” IEEE Transactions on Pattern Analysis and Machine Intelligence, vol.37, no.6, pp.1219–1232, 2015.
[5] Y. Kinoshita, S. Shiota, M. Iwahashi, and H. Kiya, “An remapping operation without tone mapping parameters for hdr images,” IEICE Transactions on Fundamentals of Electronics, Communications and Computer Sciences, vol.99, no.11, pp.1955–1961, 2016.
[6] Y. Kinoshita, S. Shiota, and H. Kiya, “Fast inverse tone mapping with reinhard’s grobal operator,” 2017 IEEE International Conference on Acoustics, Speech and Signal Processing (ICASSP), pp.1972–1976, IEEE, 2017.
[7] Y. Kinoshita, S. Shiota, and H. Kiya, “Fast inverse tone mapping based on reinhard’s global operator with estimated parameters,” IEICE Transactions on Fundamentals of Electronics, Communications and Computer Sciences,

Table 1 Experimental results for Simulation 1 (TMQI). "MEF," and "CE" indicate multi-exposure fusion and contrast enhancement, respectively.

Methods	Input image	MEF			CE			Proposed					
		[13]	[17]	[18]	HE	[22]	[23]	[13]		[17]		[18]	
								A	B	A	B	A	B
AtriumNight	0.8388	0.8514	0.8510	0.8402	0.8536	0.8236	**0.8710**	0.8579	0.8604	0.8576	0.8601	0.8449	0.8473
MtTamWest	0.7189	0.7784	0.7785	0.7718	0.7838	**0.8838**	0.8133	0.7990	0.8215	0.7964	0.8182	0.7885	0.8139
SpheronNapa	0.7239	0.7485	0.7483	0.7515	0.7423	**0.7933**	0.7734	0.7633	0.7670	0.7624	0.7660	0.7572	0.7610
Memorial	0.8404	0.8427	0.8429	0.8396	0.8381	0.7872	0.8415	0.8461	0.8522	0.8473	**0.8538**	0.8379	0.8438
Rend 11	0.7932	0.8242	0.8231	0.8142	0.8649	0.8908	**0.8994**	0.8312	0.8563	0.8303	0.8552	0.8207	0.8474
Average (5 images)	0.7830	0.8090	0.8088	0.8034	0.8165	0.8358	**0.8397**	0.8195	0.8315	0.8188	0.8307	0.8099	0.8227
Average (60 images)	0.8088	0.8151	0.8151	0.8130	0.8376	0.8248	**0.8581**	0.8294	0.8355	0.8290	0.8353	0.8236	0.8301

Table 2 Experimental results for Simulation 1 (Statistical Naturalness) "MEF," and "CE" indicate multi-exposure fusion and contrast enhancement, respectively.

Methods	Input image	MEF			CE			Proposed					
		[13]	[17]	[18]	HE	[22]	[23]	[13]		[17]		[18]	
								A	B	A	B	A	B
AtriumNight	0.1672	0.2185	0.2176	0.1644	0.3110	0.1398	**0.4060**	0.2411	0.2530	0.2398	0.2518	0.1829	0.1931
MtTamWest	0.1972	0.2326	0.2328	0.2531	0.2231	**0.7518**	0.4140	0.3027	0.3781	0.2906	0.3612	0.2931	0.3681
SpheronNapa	0.0116	0.0106	0.0105	0.0149	0.0418	**0.1694**	0.0720	0.0367	0.0430	0.0345	0.0403	0.0315	0.0368
Memorial	0.2094	0.2113	0.2122	0.1945	0.2544	0.0444	0.2890	0.2311	0.2609	0.2367	**0.2684**	0.1935	0.2209
Rend 11	0.1637	0.2425	0.2365	0.2054	0.4703	0.5784	**0.7145**	0.2555	0.3645	0.2507	0.3576	0.2129	0.3197
Average (5 images)	0.1498	0.1831	0.1819	0.1665	0.2601	0.3368	**0.3791**	0.2134	0.2599	0.2105	0.2558	0.1828	0.2277
Average (60 images)	0.2078	0.2000	0.2002	0.1903	0.3283	0.2683	**0.4496**	0.2543	0.2839	0.2528	0.2826	0.2278	0.2575

Table 3 Experimental results for Simulation 1 (CIEDE2000) "MEF," and "CE" indicate multi-exposure fusion and contrast enhancement, respectively.

Methods	Input image	MEF			CE			Proposed					
		[13]	[17]	[18]	HE	[22]	[23]	[13]		[17]		[18]	
								A	B	A	B	A	B
AtriumNight	0.000	2.872	2.816	1.628	8.769	7.536	10.127	2.231	2.511	2.208	2.490	**1.176**	1.357
MtTamWest	0.000	3.881	3.864	2.715	5.875	4.994	5.869	1.891	3.832	1.879	3.826	**1.335**	2.806
SpheronNapa	0.000	4.565	4.561	2.821	4.204	8.724	5.024	2.346	2.627	2.334	2.617	**1.472**	1.794
Memorial	0.000	2.984	2.932	3.544	6.795	9.617	9.105	1.762	2.690	**1.742**	2.682	2.443	3.213
Rend 11	0.000	3.447	3.403	2.947	7.418	7.343	8.766	2.892	5.582	2.862	5.560	**2.212**	4.827
Average (5 images)	0.000	3.550	3.515	2.731	6.612	7.643	7.778	2.224	3.448	2.205	3.435	**1.727**	2.800
Average (60 images)	0.000	3.353	3.326	2.433	7.527	7.397	8.785	2.417	3.434	2.400	3.424	**1.912**	2.839

vol.100, no.11, pp.1–3, 2017.

[8] Y.Q. Huo and X.D. Zhang, "Single image-based hdr imaging with crf estimation," 2016 International Conference On Communication Problem-Solving (ICCP), pp.1–3, IEEE, 2016.

[9] T. Murofushi, M. Iwahashi, and H. Kiya, "An integer tone mapping operation for hdr images expressed in floating point data," 2013 IEEE International Conference on Acoustics, Speech and Signal Processing (ICASSP), pp.2479–2483, IEEE, 2013.

[10] T. Murofushi, T. Dobashi, M. Iwahashi, and H. Kiya, "An integer tone mapping operation for hdr images in openexr with denormalized numbers," 2014 IEEE International Conference on Image Processing (ICIP), pp.4497–4501, IEEE, 2014.

[11] T. Dobashi, T. Murofushi, M. Iwahashi, and K. Hitoshi, "A fixed-point global tone mapping operation for hdr images in the rgbe format," IEICE Transactions on Fundamentals of Electronics, Communications and Computer Sciences, vol.97, no.11, pp.2147–2153, 2014.

[12] A.A. Goshtasby, "Fusion of multi-exposure images," Image and Vision Computing, vol.23, no.6, pp.611–618, 2005.

[13] T. Mertens, J. Kautz, and F. Van Reeth, "Exposure fusion: A simple and practical alternative to high dynamic range photography," Computer Graphics Forum, vol.28, no.1, pp.161–171, 2009.

[14] A. Saleem, A. Beghdadi, and B. Boashash, "Image fusion-based contrast enhancement," EURASIP Journal on Image and Video Processing, vol.2012, no.1, p.10, 2012.

[15] J. Wang, G. Xu, and H. Lou, "Exposure fusion based on

Table 4 Experimental results for Simulation 2 (Statistical Naturalness) "MEF," and "CE" indicate multi-exposure fusion and contrast enhancement, respectively.

Methods	Input image	MEF			CE			Proposed					
		[13]	[17]	[18]	HE	[22]	[23]	[13]		[17]		[18]	
								A	B	A	B	A	B
Arno	0.0031	0.0264	0.0243	0.0360	**0.2246**	0.0448	0.1291	0.0095	0.0947	0.0092	0.0903	0.0072	0.1200
Cave	0.0006	0.0188	0.0174	0.0527	**0.3231**	0.0034	0.0070	0.0004	0.0009	0.0004	0.0011	0.0005	0.0001
Chinese garden	0.0772	0.1076	0.1141	0.1341	**0.3460**	0.0880	0.2298	0.1044	0.2267	0.1034	0.2552	0.0904	0.1739
Corridor 1	0.0000	0.0000	0.0000	0.0000	**0.3556**	0.0000	0.0015	0.0000	0.2112	0.0000	0.2076	0.0000	0.2371
Corridor 2	0.0000	0.0085	0.0077	0.0053	**0.3031**	0.0006	0.0473	0.0001	0.0854	0.0001	0.0817	0.0000	0.1066
Estate rsa	0.0049	0.0458	0.0411	0.0411	0.4502	0.1564	**0.6606**	0.0160	0.1910	0.0149	0.1850	0.0118	0.1641
Kluki	0.2843	0.3584	0.3388	0.2889	0.3526	0.4205	**0.9720**	0.3992	0.6323	0.3852	0.6151	0.3731	0.6129
Laurenziana	0.4360	0.3424	0.3261	0.3799	0.3967	0.6133	**0.9213**	0.5328	0.8753	0.5232	0.8799	0.4939	0.8344
Lobby	0.0006	0.0037	0.0032	0.0043	0.4276	0.0031	0.0206	0.0008	0.4635	0.0008	**0.4733**	0.0008	0.4448
Mountains	0.2867	0.0622	0.0563	0.0692	0.4029	0.6072	**0.8669**	0.2741	0.1514	0.2669	0.1483	0.3588	0.1774
Ostrow tumski	0.0055	0.0199	0.0176	0.0489	0.1545	0.0636	0.1955	0.0119	0.3626	0.0115	0.3478	0.0117	**0.4887**
Window	0.0020	0.0068	0.0065	0.0070	0.2777	0.0133	0.0397	0.0043	0.3515	0.0042	0.3401	0.0036	**0.4653**

Table 5 Experimental results for Simulation 2 (CIEDE2000) "MEF," and "CE" indicate multi-exposure fusion and contrast enhancement, respectively.

Methods	Input image	MEF			CE			Proposed					
		[13]	[17]	[18]	HE	[22]	[23]	[13]		[17]		[18]	
								A	B	A	B	A	B
Arno	0.000	8.621	8.601	10.319	12.433	8.593	12.896	3.317	12.391	3.293	12.365	**2.289**	13.228
Cave	0.000	15.858	15.826	19.969	31.178	6.045	9.757	1.353	31.862	**1.290**	31.881	1.297	32.508
Chinese garden	0.000	11.954	11.882	10.922	16.282	13.556	15.954	2.594	15.706	2.470	15.660	**2.294**	15.231
Corridor 1	0.000	3.794	3.785	2.551	40.235	6.738	19.344	1.347	36.950	1.335	36.948	**0.944**	37.685
Corridor 2	0.000	22.179	22.164	19.810	30.185	9.368	24.636	3.377	27.568	3.364	27.558	**1.812**	28.086
Estate rsa	0.000	11.064	11.025	8.969	17.134	14.656	21.380	3.916	15.092	3.877	15.071	**2.999**	13.963
Kluki	0.000	11.081	11.017	5.740	3.103	12.403	12.160	2.457	5.412	2.389	5.356	**1.870**	4.945
Laurenziana	0.000	10.809	10.789	7.449	6.372	9.849	11.054	2.097	7.696	2.032	7.667	**1.711**	7.269
Lobby	0.000	8.552	8.520	8.232	33.087	7.074	16.938	1.339	31.463	1.312	31.457	**1.022**	31.529
Mountains	0.000	6.066	6.069	6.325	13.475	6.246	9.603	1.248	4.308	1.239	4.308	**0.852**	4.131
Ostrow tumski	0.000	7.077	7.032	8.297	9.976	8.562	11.694	2.114	15.677	2.089	15.667	**1.795**	17.287
Window evaluative	0.000	5.077	5.057	4.537	22.795	6.531	8.342	2.246	21.415	2.230	21.422	**1.477**	21.859

sparse coding in pyramid transform domain," Proceedings of the 7th International Conference on Internet Multimedia Computing and Service, ICIMCS '15, New York, NY, USA, pp.4:1–4:4, ACM, 2015.
[16] Z. Li, J. Zheng, Z. Zhu, and S. Wu, "Selectively detail-enhanced fusion of differently exposed images with moving objects," IEEE Transactions on Image Processing, vol.23, no.10, pp.4372–4382, 2014.
[17] T. Sakai, D. Kimura, T. Yoshida, and M. Iwahashi, "Hybrid method for multi-exposure image fusion based on weighted mean and sparse representation," 2015 23rd European Signal Processing Conference (EUSIPCO), pp.809–813, EURASIP, 2015.
[18] M. Nejati, M. Karimi, S.M.R. Soroushmehr, N. Karimi, S. Samavi, and K. Najarian, "Fast exposure fusion using exposedness function," 2017 International Conference on Image Processing (ICIP), pp.2234–2238, IEEE, 2017.
[19] F. Dufaux, P.L. Callet, R. Mantiuk, and M. Mrak, High Dynamic Range Video, From Acquisition, to Display and Applications, Elsevier Ltd., 2016.
[20] H. Youngquing, Y. Fan, and V. Brost, "Dodging and burning inspired inverse tone mapping algorithm," Journal of Computational Information Systems, vol.9, no.9, pp.3461–3468, 2013.
[21] E. Reinhard, M. Stark, P. Shirley, and J. Ferwerda, "Photographic tone reproduction for digital images," ACM Transactions on Graphics (TOG), vol.21, no.3, pp.267–276, 2002.
[22] K. Zuiderveld, "Contrast limited adaptive histograph equalization," Graphics gems IV, pp.474–485, Academic Press Professional, Inc., 1994.
[23] X. Wu, X. Liu, K. Hiramatsu, and K. Kashino, "Contrast-accumulated histogram equalization for image enhnacement," 2017 International Conference on Image Processing (ICIP), pp.3190–3194, IEEE, 2017.
[24] H. Yeganeh and Z. Wang, "Objective quality assessment of tone mapped images," IEEE Transactions on Image Processing, vol.22, no.2, pp.657–667, 2013.
[25] G. Sharma, W. Wu, and E.N. Dalal, "The ciede2000 color-difference formula: Implementation notes, supplementary test data, and mathematical observations," Color research and application, vol.30, no.1, pp.21–30, 2005.
[26] "Github - openexr." https://github.com/openexr/.
[27] "High dynamic range image examples." http://www.anyhere.com/gward/hdrenc/pages/originals.html.
[28] "easyhdr." https://www.easyhdr.com/.


(a) Mertens [13]

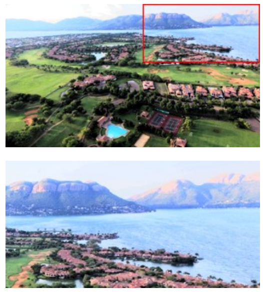
(b) HE


(c) CACHE [23]

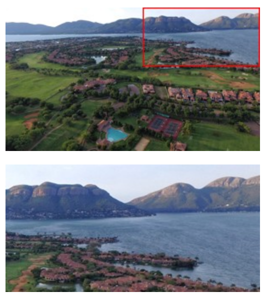
(d) Proposed (A) with [13]


(e) Proposed (B) with [13]

Fig. 6 Images I' generated from image "Estate rsa" (top) and zoom-in views of their upper right corner (bottom).

Yuma Kinoshita received his B.Eng. and M.Eng. degrees from Tokyo Metropolitan University, Japan, in 2016 and 2018, respectively. From 2018, he has been a Ph.D. student at Tokyo Metropolitan University. He received IEEE ISPACS Best Paper Award in 2016. His research interests are in the area of image processing. He is a student member of IEEE and IEICE.

Sayaka Shiota received the B.E., M.E. and Ph.D. degrees in intelligence and computer science, Engineering and engineering simulation from Nagoya Institute of Technology, Nagoya, Japan in 2007, 2009 and 2012, respectively. From February 2013 to March 2014, she had worked at the Institute professor. In April of 2014, she joined Tokyo Metropolitan University as an Assistant Professor. Her research interests include statistical speech recognition and speaker verification. She is a member of the Acoustical Society of Japan (ASJ), the IEICE, and the IEEE.

Hitoshi Kiya received his B.Eng. and M.Eng. degrees from Nagaoka University of Technology, Japan, in 1980 and 1982, respectively, and his D.Eng. degree from Tokyo Metropolitan University in 1987. In 1982, he joined Tokyo Metropolitan University as an Assistant Professor, where he became a Full Professor in 2000. From 1995 to 1996, he attended the University of Sydney, Australia as a Visiting Fellow. He was/is the Chair of IEEE Signal Processing Society Japan Chapter, an Associate Editor for IEEE Trans. Image Processing, IEEE Trans. Signal Processing and IEEE Trans. Information Forensics and Security, respectively. He also serves/served as the President of IEICE Engineering Sciences Society (ESS), the Editor-in-Chief for IEICE ESS Publications, and the President-Elect of APSIPA, His research interests are in the area of signal and image processing including multirate signal processing, and security for multimedia. He received the IWAIT Best Paper Award in 2014 and 2015, IEEE ISPACS Best Paper Award in 2016, the ITE Niwa-Takayanagi Best Paper Award in 2012, the Telecommunications Advancement Foundation Award in 2011, the IEICE ESS Contribution Award in 2010, and the IEICE Best Paper Award in 2008. He is a Fellow Member of IEEE, IEICE and ITE.